RSC Advances

PAPER

View Article Online
View Journal | View Issue

Cite this: *RSC Adv.*, 2017, **7**, 30310

First-principles study on structural, electronic, vibrational and thermodynamic properties of $Sr_{10}(PO_4)_6X_2$ (X = F, Cl, Br)

Zhihong Yuan,[a] Tao Gao,*[ab] Yuanlei Zheng,[a] Shenggui Ma,[a] Mingli Yang[ab] and Piheng Chen*[c]

A theoretical investigation on the structural stability, electronic, vibrational, and thermodynamic properties of the strontium apatites $Sr_{10}(PO_4)_6X_2$ (X = F, Cl, Br) is systematically conducted by the first-principles calculations. Results of cohesive energies and formation enthalpies suggest that the thermal stability of strontium apatites decreases from $Sr_{10}(PO_4)_6F_2$ (Sr-FAP) to $Sr_{10}(PO_4)_6Cl_2$ (Sr-ClAP) and further to $Sr_{10}(PO_4)_6Br_2$ (Sr-BrAP); such a tendency is also be observed with regard to the band gaps. Using linear-response approach, the detailed vibrational properties of $Sr_{10}(PO_4)_6X_2$ (X = F, Cl, Br) are obtained. According to the calculated phonon dispersions, it is concluded that strontium apatites $Sr_{10}(PO_4)_6X_2$ (X = F, Cl, Br) are dynamically stable, and the phonon behaviors are generally similar to these apatites, but most of the vibrational frequencies decrease from Sr-FAP, Sr-ClAP to Sr-BrAP. The assignment of the vibrational modes at the gamma point demonstrate that all the silent mode B_g, B_u and E_{2u} are affected and the only optically active mode involved is the Raman active mode E_{2g} with the replacement of larger Cl^- and Br^- for F^-. The results calculated with the quasi-harmonic approximation (QHA) show that $Sr_{10}(PO_4)_6X_2$ (X = F, Cl, Br) exhibits similar but slightly different behaviors in terms of its thermodynamic properties, which is expected because the halogen atoms F, Cl and Br are in the same VIIA group. Significantly, all the present calculation results are satisfactory compared to the existing experimental and theoretical results.

Received 18th April 2017
Accepted 5th June 2017

DOI: 10.1039/c7ra04359g

rsc.li/rsc-advances

1. Introduction

Phosphate-bearing apatites with the general formula $M_{10}(PO_4)_6X_2$ (M = Ca, Sr, Ba, Pb, *etc.*; X = F, Cl, Br, OH, *etc.*) have been attracting considerable attention from scientists due to their significance in many fields, which vary from geochronology to environment remediation and optoelectronic as well as biomaterials and medical sciences.[1–7] Calcium apatites which are the typical representatives of the apatite family have been the most extensively investigated, due to their proverbial industrial and biological applications.[8–14] Furthermore, researchers have been constantly discussing the various ionic substitutions in calcium apatites[15–20] for the sake of better applications of apatites.

Strontium (Sr) is one of the most common substituents in the apatite structure. The presence and behavior of Sr in apatite compounds are of great significance in geology, biology and materials science, and some studies have paid more attention to the $Ca_{10-x}Sr_x(PO_4)_6X_2$ (X = F, Cl) apatites.[21–23] In this paper, we focus on the Sr-richest apatites $Sr_{10}(PO_4)_6X_2$ (X = F, Cl, Br) which as the Sr end-member apatites have many practical applications. Firstly, $Sr_{10}(PO_4)_6X_2$ (X = F, Cl, Br) are well-known hosts for functional rare earth ions with subsequent applications as fluorescent and laser materials.[24–30] Secondly, $Sr_{10}(PO_4)_6F_2$ (Sr-FAP) is of interest in biological fields because of the ready entry of Sr into the food chain and its subsequent incorporation in bone.[31–34] Thirdly, as the member of apatite family, $Sr_{10}(PO_4)_6X_2$ (X = F, Cl, Br) are considered to be suitable for nuclear waste storage, such as the glass encapsulated $Sr_{10}(PO_4)_6Cl_2$ (Sr-ClAP) can immobilize most of the radwaste elements in the composite matrix.[35]

There are some investigations have been carried on the crystal $Sr_{10}(PO_4)_6X_2$ (X = F, Cl, Br). The crystal structures of $Sr_{10}(PO_4)_6X_2$ (X = F, Cl, Br) were determined with X-ray diffraction.[36–38] Several groups[15,39–42] have studied the infrared (IR) and Raman (R) spectra of $Sr_{10}(PO_4)_6X_2$ (X = F, Cl, Br). The phase transitions and thermal expansion of Sr-FAP and Sr-ClAP were studied by high temperature X-ray diffraction and differential thermal analysis.[43,44] The results indicate Sr-FAP and Sr-ClAP have large thermal expansion coefficient and there are not any phase transformations for Sr-FAP and Sr-ClAP in

[a]*Institute of Atomic and Molecular Physics, Sichuan University, Chengdu, 610065, China. E-mail: gaotao@scu.edu.cn*

[b]*Key Laboratory of High Energy Density Physics and Technology of Ministry of Education, Sichuan University, Chengdu, 610064, China*

[c]*Science and Technology on Surface Physics and Chemistry Laboratory, Mianyang, 621907, China. E-mail: chenph@live.cn*

temperature interval 298–1723 K. The formation enthalpies of Sr-FAP and Sr-ClAP were given at the standard of 298 K and 1 bar.[45–47] Specially, the heat capacity and enthalpy increments of Sr-ClAP were measured by Hrudananda Jena *et al.*[35,48,49] Furthermore, the thermodynamics functions of Sr-ClAP were computed by least-squares fitting method from the measured enthalpy increments and compared with the $Ca_{10}(PO_4)_6Cl_2$ and $Ba_{10}(PO_4)_6Cl_2$, which indicate that the specific heat capacity of the alkaline earth chloroapatites increases in the order barium < strontium < calcium and the alkaline earth chloroapatites can withstand decay heat of the radio nuclides without decomposition or degradation.[49] Theoretically, the electronic properties and elastic constants of $Sr_{10}(PO_4)_6X_2$ (X = F, Cl, Br) were calculated using density functional theory (DFT) with the generalized gradient approximation (GGA) functional.[50] Besides, the elastic constants of Sr-FAP and Sr-ClAP also were predicted using the program GULP.[51]

As mentioned above, there is presently a dearth of vibrational and thermodynamic information for $Sr_{10}(PO_4)_6X_2$ (X = F, Cl, Br). However, the thermodynamic functions such as enthalpy, heat capacity and entropy for $Sr_{10}(PO_4)_6X_2$ (X = F, Cl, Br) are very important as the apatites (especially the $Sr_{10}(PO_4)_6Cl_2$) becoming more and more important for radioactive waste immobilization. Computational prediction for these properties is of interest and motivates us to acquire further knowledge to define better applications of these apatites. The aim of this paper is to provide the first systematic study of the structural, electronic, vibrational and thermodynamic properties of the strontium apatites $Sr_{10}(PO_4)_6X_2$ (X = F, Cl, Br) from first-principles calculations.

The remainder of this paper is structured as follows: in Section 2, the Computational details are briefly described. Section 3 is devoted to Results and discussions, we present the structural, electronic, vibrational and thermodynamic properties of $Sr_{10}(PO_4)_6X_2$ (X = F, Cl, Br). Finally, the Conclusions of the present work are given in Section 4.

2. Computational details

In the present work, the first-principles calculations based on the DFT[52] are performed by the Vienna Ab initio Simulation Package (VASP) code.[53] The local density approximation (LDA) with Ceperley–Alder (CA) functional[54] is applied to describe the exchange correlation energy, the valence electron configurations for these elements are Sr $4s^24p^65s^2$, P $3s^23p^3$, O $2s^22p^4$, F $2s^22p^5$, Cl $3s^23p^5$ and Br $4s^24p^5$, respectively. The primitive cells of $Sr_{10}(PO_4)_6X_2$ (X = F, Cl, Br), which contain 42 atoms are chosen in all our calculations in order to reduce the computational cost. The energy cutoff of 520 eV is chosen to determine the number of plane waves in expansion, the *k*-point mesh is set at $2\pi \times 0.04$ Å^{-1} for samplings in the irreducible edge of Brillouin zone (BZ)[55] during our calculations. Both the kinetic-energy cutoff and *k*-point sampling have been tested to be sufficient for convergence. Besides, the total energy is converged to 10^{-7} eV and the force acting on each atom is converged to less than 0.01 eV Å^{-1} throughout the present calculations. The equilibrium structures of $Sr_{10}(PO_4)_6X_2$ (X = F, Cl, Br) are obtained by minimizing the total energy with respect to the fully optimized of cell volume, cell shape and atomic positions in primitive cells.

The phonon calculations are performed by the linear response approach as implemented in the PHONOPY code,[56] with VASP code used as the computational engine. The vibrational properties including the phonon dispersion curves and phonon density of states, Born effective charge tensor and associated longitudinal optical and transverse optical (LO–TO) splitting of optical modes, as well as the phonon frequencies at the Brillouin zone center are obtained in the framework of the density functional perturbation theory (DFPT). Thereafter, some phonon related thermodynamic properties such as Helmholtz free energy *F*, internal energy *E*, entropy *S* and specific heat C_V (C_P) are predicted within the QHA.

3. Results and discussions

3.1. Structural properties and phase stability

The apatites $Sr_{10}(PO_4)_6X_2$ (X = F, Cl, Br) have the fairly complex hexagonal crystal structures with the space group $P6_3/m$ (no. 176). The models are illustrated in Fig. 1, which are composed of six PO_4 groups surrounded by ten Sr atoms with two X ions located along the *c* axis. Of which ten Sr atoms occupy two different crystallographic symmetry sites 4f and 6h. The PO_4 groups occupy 6h sites, while the oxygen atoms have three unique environments. The very difference for these apatites is the positions of halogen atoms. The F atoms lie at the $z = 0.25$ and $z = 0.75$, occupy the 2a positions in Sr-FAP, whereas the Cl and Br atoms lie at $z = 0$ and $z = 1/2$, occupy the 2b positions in Sr-ClAP and Sr-BrAP.

In the first step, the crystal structures of $Sr_{10}(PO_4)_6X_2$ (X = F, Cl, Br) are fully optimized by minimizing the total energy. The obtained results after relaxation are summarized in Table 1 and in comparison with the experimental[36–38] and other theoretical values.[50] Obviously, the optimized structure parameters in our calculations with LDA underestimate by 1–2% with respect to the experiment values, while the theoretical values calculated with GGA overestimate within 1–2%, which due to the general feature of DFT that LDA underestimate and GGA overestimate the structure parameters. Therefore, the optimized structures are sufficient to allow us to make a further study of the electronic, vibrational and thermodynamic properties of these apatites. After analysis, we note the replacement of F by Cl and

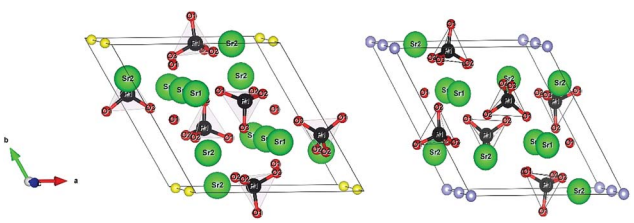

Fig. 1 The crystal structures of $Sr_{10}(PO_4)_6X_2$ (X = F, Cl, Br), the atomic species are labeled on the balls. And the yellow balls represent the F atoms, blue balls represent the Cl or Br atoms (the figures are generated by the VESTA code[57]).

Table 1 Optimized and experimental structural parameters for Sr-FAP, Sr-ClAP and Sr-BrAP apatites

	Lattice parameters (Å)				
Apatite	*a*	*c*	*V* (Å^3)	*c*/*a*	Ref.
Sr-FAP	9.568	7.183	569.47	0.751	This work
	9.678	7.275	590.11	0.752	Expt[a]
	9.841	7.365	617.80	0.748	Cal.[d]
Sr-ClAP	9.711	7.085	578.63	0.730	This work
	9.859	7.205	606.58	0.731	Expt[b]
	10.015	7.258	630.45	0.725	Cal.[d]
Sr-BrAP	9.796	7.101	590.15	0.725	This work
	9.972	7.214	621.26	0.723	Expt[c]
	10.108	7.272	643.36	0.719	Cal.[d]

[a] Ref. 36. [b] Ref. 37. [c] Ref. 38. [d] Ref. 50.

Br causes the cell volumes of the apatites to expand, but leading to a decreased *c*/*a* ratio of the unit cell, which can be explained by the fact that the halogen ionic radius increased from F^- to Br^-.

The stability for apatites is very important to control sintering or thermal processing conditions for the design and preparation of apatite ceramics. In order to determine the relative stability of $Sr_{10}(PO_4)_6X_2$ (X = F, Cl, Br) apatites, the cohesive energy and formation enthalpy of $Sr_{10}(PO_4)_6X_2$ (X = F, Cl, Br) are calculated by the following definitions:

$$E_c(Sr_{10}(PO_4)_6X_2) = E(Sr_{10}(PO_4)_6X_2) - 10E_{iso}(Sr) - 6E_{iso}(P) - 24E_{iso}(O) - 2E_{iso}(X)$$

$$\Delta H(Sr_{10}(PO_4)_6X_2) = E(Sr_{10}(PO_4)_6X_2) - 10E(Sr) - 6E(P) - 12E(O_2) - E(X_2)$$

where $E_c(Sr_{10}(PO_4)_6X_2)$ and $\Delta H(Sr_{10}(PO_4)_6X_2)$ are the cohesive energy and formation enthalpy of $Sr_{10}(PO_4)_6X_2$ (X = F, Cl, Br). $E(Sr_{10}(PO_4)_6X_2)$ is the total energy of per $Sr_{10}(PO_4)_6X_2$ formula; $E_{iso}(Sr)$, $E_{iso}(P)$, $E_{iso}(O)$ and $E_{iso}(X)$ are the energies of an isolated atom for each element. $E(Sr)$, $E(P)$, $E(O_2)$ and $E(X_2)$ are the energies of strontium, white phosphorus, O_2 gas and halogen gas, respectively. More negative formation enthalpy and cohesive energy generally correspond to a better stability.

Table 2 Calculated and experimental cohesive energies E_c (eV) and formation enthalpies ΔH (kJ mol^{-1}) of per atom for Sr-FAP, Sr-ClAP and Sr-BrAP apatites

Apatite	X^- ionic radii, Å	E_c, eV	ΔH, kJ mol^{-1}	Ref.
Sr-FAP	1.33	−6.74	−314.3	This work
			−323.9	Expt[a]
			−332.9	Cal.[c]
Sr-ClAP	1.81	−6.65	−304.0	This work
			−315.1	Expt[b]
			−323.1	Cal.[c]
Sr-BrAP	1.96	−6.60	−300.8	This work
			−317.2	Cal.[c]

[a] Ref. 45 and 46. [b] Ref. 47. [c] Ref. 50.

The calculated cohesive energies and formation enthalpies of these apatites are tabulated in Table 2, along with the experimental data and other published. Apparently, our calculated formation enthalpies of these apatites are agree well with the experimental values.[45–47] The negative cohesive energies and formation enthalpies show these strontium apatites are stable. Compared with the results given by Michael Kocher,[50] we find that GGA could obtain more negative cohesive energy and formation enthalpy, but the LDA opposite. Further analysis, the stability of these apatites is related to the halogen anion radius and decreases in the following order Sr-FAP > Sr-ClAP > Sr-BrAP, which is reflected by the more negative cohesive energy and formation enthalpy of Sr-FAP than that of Sr-ClAP and Sr-BrAP. Such a tendency has been observed in recent publications of calcium apatites[12] and barium apatites.[16]

3.2. Electronic structure

Fig. 2 shows the calculated energy band structure of each apatite along the same high symmetry reciprocal space path. The Fermi level (E_f) is chosen to align to zero and expressed by a dash line. The main features of the band structures are common to each apatite. All these apatites are insulator materials and characterized by an indirect band gap. Table 3 provides our calculated band gaps and other theoretical values for each apatite, it is observed whether our results or the values given by Michael Kocher,[50] the band gap values decrease from Sr-FAP to Sr-ClAP to Sr-BrAP. As far as we know, for some have been studied apatites,[9,12,16,20] (such as calcium apatites, barium apatites and cadmium apatites) the band gaps decrease with the reduction of X ion electronegativity. In addition, as already noted that DFT predictions always underestimate the true band gap so the real values may be somewhat higher than calculated here.

Fig. 3 plots the total density of states (TDOS) and the partial densities of states for each apatite. The DOSs of these apatites are very similar along with slight differences as with the band structures. The DOSs below Fermi energy in the energy range of −10 eV to 0 eV are described by four main peaks (A–D). Peak A mostly derived from O 2p and P 3s states with some O 2s contributions, while peak B is dominated by O 2p and P 3p states. As for peaks C and D are mainly composed of O 2p states and the peak C has receive approximately 10% of their value from the X p states. The conduction band is chiefly contributed

Table 3 Calculated band gap E_g (eV) for Sr-FAP, Sr-ClAP and Sr-BrAP apatites

Apatite	Sr-FAP	Sr-ClAP	Sr-BrAP
This work	5.42	5.27	5.11
Cal.[a]	5.21	5.08	4.93

[a] Ref. 50.

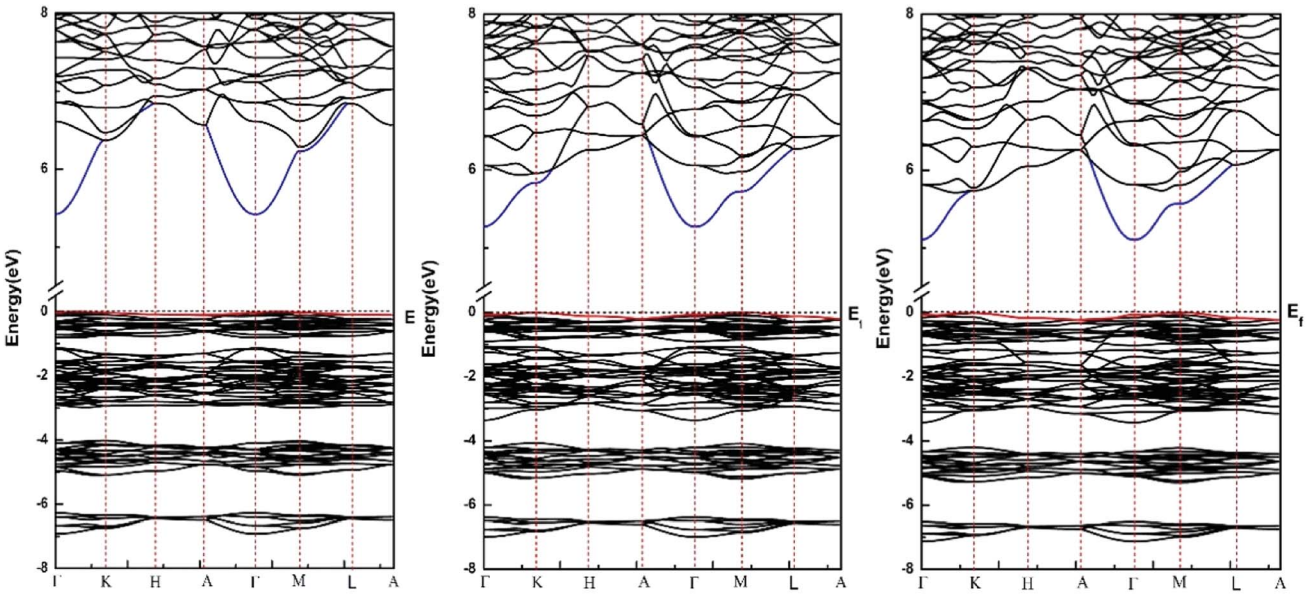

Fig. 2 Calculated band structures for Sr-FAP, Sr-ClAP and Sr-BrAP apatites.

from Sr 4d states with some mixing of O 2s, O 2p and F p states. There are also three main peaks (1–3) below −10 eV for $Sr_{10}(PO_4)_6X_2$ (X = F, Cl, Br). Of these peaks, the peak 1 is primarily from O 2s and P 3s states, while the peak 2 is mainly from the O 2s states and P 3p states. Another significant peak 3 for these apatites principally made up by Sr 4p with the minor

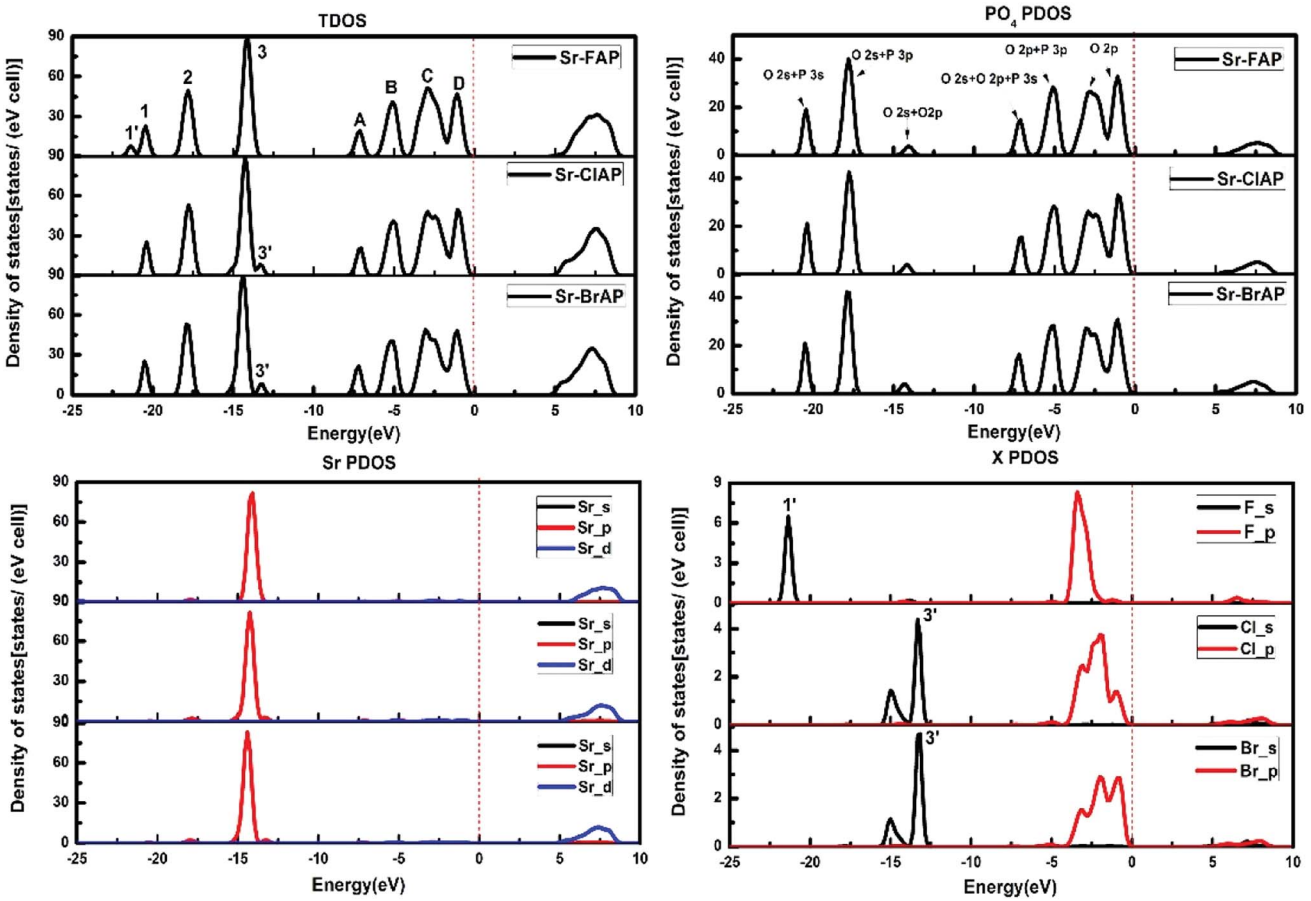

Fig. 3 Total density of states (TDOS) and partial density of states (PDOS) for Sr-FAP, Sr-ClAP and Sr-BrAP apatites.

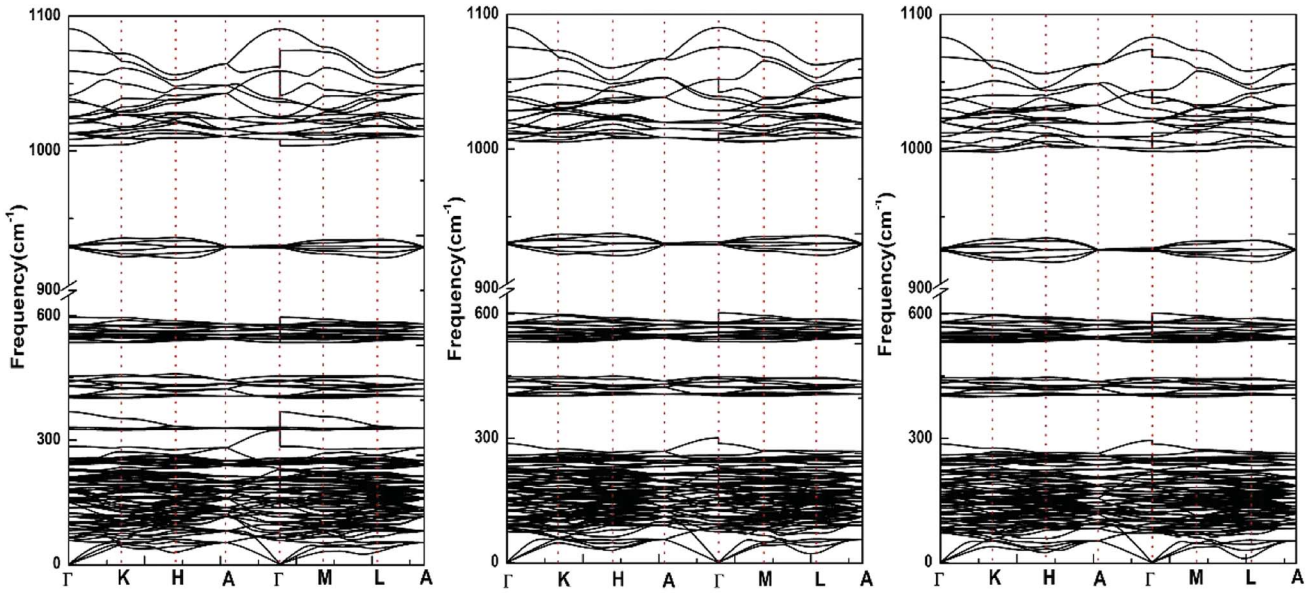

Fig. 4 Calculated phonon dispersion curves (including LO–TO splitting) for Sr-FAP, Sr-ClAP and Sr-BrAP apatites.

contribution of O 2s and O 2p states, while for Sr-ClAP and Sr-BrAP the Cl 3s and Br 4s states also contribute to the peak 3. Furthermore, from the X PDOS in Fig. 3, we note about −15 eV there is a peak 3′ which also comes from Cl 3s (Br 4s) states, and Sr-FAP has a small peak 1′ at about −21 eV from its F s states. The similar phenomena are also reported in the recent publications of calcium apatites[12] and barium apatites[16] calculated with the DFT.

3.3. Vibrational properties

3.3.1. Phonon dispersion curves and phonon density of states. The available experimental and theoretical data are very limited for vibrational properties of $Sr_{10}(PO_4)_6X_2$ (X = F, Cl, Br), W. Klee and G. Engel[15] have given the infrared spectra of various apatites $M_5(PO_4)_3$ X (M = Ca, Sr, Cd, Ba, Pb; X = F, OH, CI, Br) in 1970, then several groups[40–42] have pay attention to the Raman spectra of Sr-FAP. Recently, P. V. Balachandran *et al.*[58] confirmed that Sr-FAP is dynamically stable through searching the low-energy frequencies at the Γ-point. Herein, the detailed vibrational properties of each apatite are investigated by using the DFPT. Fig. 4 presents the calculated phonon dispersions curves (including the LO–TO splitting for infrared active modes) along the high symmetry directions of these apatites at their theoretical equilibrium volumes. It is well known that phonon dispersion curves can give a criterion for the crystal stability. Obviously, there is no imaginary phonon frequency observed throughout the BZ in Fig. 4, which suggests that strontium apatites $Sr_{10}(PO_4)_6X_2$ (X = F, Cl, Br) are dynamically stable. Fig. 4 also reveals that the phonon behaviors are generally similar for these apatites, but we find the maximum values of these phonon curves are higher for the Sr-FAP than that of Sr-ClAP and Sr-BrAP, and most of the vibrational frequencies decrease from Sr-FAP, Sr-ClAP to Sr-BrAP which is caused by the different atomic mass of F, Cl and Br (F < Cl < Br).

Since all the primitive cells of hexagonal Sr-FAP, Sr-ClAP and Sr-BrAP contain 42 atoms, the complete phonon spectrum for each apatite consists 126 dispersion curves, of which 3 are acoustical modes and the remaining 123 are optical modes. According to the standard group-theoretical analysis based on the $P6_3/m$ space group, the Sr-FAP yields the optical phonon modes at the Γ point, as following:

$$\Gamma_{opt} = 12A_g + 8E_{1g} + 13E_{2g} + 8A_u + 12E_{1u} + 12B_u + 9B_g + 8E_{2u}$$

The Sr-ClAP and Sr-BrAP yield the optical phonon modes at the Γ point, as following:

$$\Gamma_{opt} = 12A_g + 8E_{1g} + 12E_{2g} + 8A_u + 12E_{1u} + 13B_u + 8B_g + 9E_{2u}$$

Of these modes, A_g, E_{1g} and E_{2g} are corresponding to Raman active modes, whereas the A_u and E_{1u} are infrared active modes, B_g, B_u and E_{2u} are silent modes. The A and E modes are singly and doubly degenerate modes, respectively.

Interestingly, with the replacement of larger Cl^- and Br^- for F^-, all the silent modes B_g, B_u and E_{2u} are affected and the only optically active modes involved is the Raman active mode E_{2g}, which can be explained by the different Wyckoff sites of X (X = F, Cl, Br) ions in theirs apatite structures.

Fig. 5 illustrates the phonon total density of state and the phonon partial density of states for each apatite. It is distinctly for these apatites that the modes beyond 350 cm^{-1} up to 1100 cm^{-1} are contributed from PO_4 group vibrations. And since these selected apatites differ only in X atoms, their high-frequency spectra are naturally very similar. Some characteristic differences among these apatites can be found at the low frequencies (<350 cm^{-1}). The massive modes of these apatites below 300 cm^{-1} involve the vibrations of all bonds are the major contributions to thermodynamics. But owing to the fact that

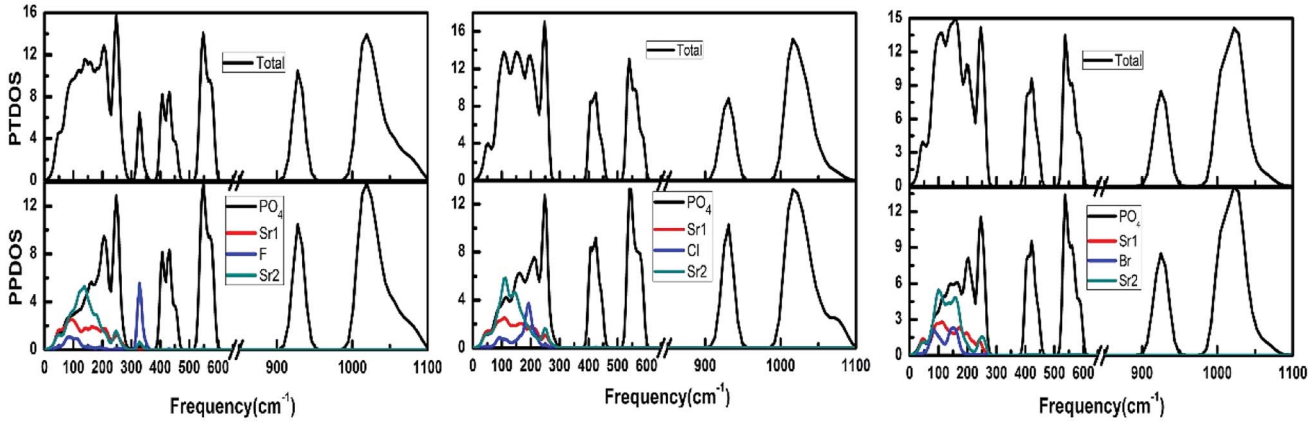

Fig. 5 Phonon total density of states (PTDOS) and phonon partial density of states (PPDOS) for Sr-FAP, Sr-ClAP and Sr-BrAP apatites.

Table 4 Diagonal component of Born effective charge tensor Z^* for Sr-FAP, Sr-ClAP and Sr-BrAP apatites

		Sr-FAP		Sr-ClAP		Sr-BrAP	
Site	Atom	$Z^*_{xx}\left(Z^*_{yy}\right)$	Z^*_{zz}	$Z^*_{xx}\left(Z^*_{yy}\right)$	Z^*_{zz}	$Z^*_{xx}\left(Z^*_{yy}\right)$	Z^*_{zz}
4f	Sr_1	2.408	2.630	2.485	2.555	2.505	2.544
6h	Sr_2	2.562	2.494	2.500	2.702	2.495	2.692
6h	P	3.310	3.109	3.386	3.181	3.410	3.217
6h	O_1	−2.010	−1.423	−2.017	−1.413	−2.025	−1.406
6h	O_2	−1.935	−1.334	−2.045	−1.321	−2.087	−1.325
12i	O_3	−1.498	−2.181	−1.563	−2.187	−1.578	−2.197
2a	F	−1.609	−0.714				
2b	Cl			−1.068	−1.440		
2b	Br					−0.932	−1.447

atomic mass of F is lighter than that of Cl and Br, the frequencies in the 300–350 cm^{-1} region are associated with the Sr–F bond only. In addition, we find the low frequencies increased with the increase in the atomic mass (F < Cl < Br).

3.3.2. The LO–TO splitting. It is generally known that LO–TO splitting can be considered into the dynamical matrix by a non-analytical contribution, which depends on the Born effective charge (BEC) tensor and the dielectric constant.[59–61] In the present work, BEC tensor (Z^*) and macroscopic static dielectric constant tensor (ε) of each apatite are calculated through the DFPT. The calculated diagonal elements Z^* for 7 non-equivalent atoms are given in Table 4. There is a small deviation from charge neutrality which is smaller than 0.022 electrons per unit cell suggesting that our results are well converged. Since the hexagonal symmetry of crystals, the three diagonal elements Z^*_{xx}, Z^*_{yy} and Z^*_{zz} for each atom possess two independent components $\left(Z^*_{xx} = Z^*_{yy}\right)$. Clearly, the Z^* diagonal components are close to the nominal ionic values of Sr (+2), O

Table 5 Diagonal component of macroscopic static dielectric tensor ε for Sr-FAP, Sr-ClAP and Sr-BrAP apatites

Apatite	Sr-FAP	Sr-ClAP	Sr-BrAP
$\varepsilon_{xx}(\varepsilon_{xx})$	2.92	3.09	3.15
ε_{zz}	2.91	3.11	3.19

Table 6 The calculated Raman active (R) modes at the Γ point for Sr-FAP, Sr-ClAP, Sr-BrAP apatites, and corresponding experimental Raman active data of Sr-FAP (unit: cm^{-1})

	Sr-FAP		Sr-ClAP	Sr-BrAP
Modes	This work	Expt[a]	This work	This work
E_{1g}	58.0		73.6	76.7
	97.1		98.9	98.2
	152.2		150.6	151.3
	204.8		198.8	192.4
	256.0		252.1	247.1
	405.3	421	405.3	403.5
	556.4	580	556.5	555.7
	1012.7	1027	1019.5	1020.2
E_{2g}	73.4		86.0	84.4
	101.4		109.1	105.4
	149.7		152.4	148.0
	176.2		172.6	165.4
	202.2		191.5	191.0
	241.8		247.5	250.6
	326.5			
	428.9	442	422.8	421.8
	546.6	572	545.5	543.6
	579.5	601	579.2	579.0
	929.8	951	931.2	926.8
	1013.3	1028	1006.3	998.4
	1025.5	1037	1028.5	1022.9
A_g	121.5		107.9	99.5
	150.4		139.4	136.1
	181.8		169.0	159.2
	191.5		179.6	180.4
	210.7		219.5	218.8
	248.6		244.8	246.2
	431.1	444	424.1	423.8
	557.1	580	554.5	551.0
	571.5	592	576.5	578.6
	928.3	951	929.2	925.3
	1024.3	1041	1013.6	1006.1
	1038.9	1054	1037.1	1030.1

[a] Ref. 42.

Table 7 The calculated and corresponding experimental infrared active (IR) data and LO–TO splitting at the Γ point for Sr-FAP, Sr-ClAP, Sr-BrAP apatites (unit: cm^{-1})

	Sr-FAP			Sr-ClAP			Sr-BrAP		
	This work			This work			This work		
Modes	LO	TO	Expt[a]	LO	TO	Expt[a]	LO	TO	Expt[a]
$E_{1u}(1)$	86.4	80.9		83.1	79.9		72.9	71.1	
$E_{1u}(2)$	157.7	157.2		145.2	137.1		136.3	122.5	
$E_{1u}(3)$	199.7	172.7		183.4	168.3		160.1	158.3	
$E_{1u}(4)$	221.0	203.6		199.1	187.2		183.2	170.6	
$E_{1u}(5)$	274.7	249.6		231.2	208.2		218.9	188.1	
$E_{1u}(6)$	356.7	331.3		291.9	258.4		292.2	259.7	
$E_{1u}(7)$	441.2	441.1	458	436.9	436.3	459	436.3	434.4	458
$E_{1u}(8)$	548.7	543.8	570	544.9	539.1	565	542.6	536.1	562
$E_{1u}(9)$	584.4	567.0	590	584.0	569.2	591	584.2	569.7	593
$E_{1u}(10)$	929.0	928.2	949	930.4	928.9	949	926.2	924.4	945
$E_{1u}(11)$	1050.0	1008.5	1026	1044.4	1007.4	1028	1035.0	1000.6	1024
$E_{1u}(12)$	1094.3	1059.3	1075	1090.7	1052.0	1069	1083.2	1044.0	1061
$A_u(1)$	73.7	65.3		91.6	91.4		77.6	77.5	
$A_u(2)$	123.8	123.5		124.2	123.7		120.2	118.5	
$A_u(3)$	142.1	137.0		160.9	150.6		153.8	144.3	
$A_u(4)$	250.6	226.3		238.4	225.4		227.4	220.4	
$A_u(5)$	299.6	254.5		298.4	243.1		293.0	235.8	
$A_u(6)$	444.8	443.6	458	445.4	443.6	459	443.8	441.4	458
$A_u(7)$	561.8	535.2	570	557.4	533.2	565	555.0	533.2	562
$A_u(8)$	1080.9	1003.7	1026	1083.4	1011.4	1028	1081.0	1012.1	1024

[a] Ref. 15.

(−2), P (+3), F (−1), Cl (−1), Br (−1), which confirm the ionic character of these apatites from a chemical point of view. Table 5 presents the calculated diagonal elements of ε. Due to the symmetry of the crystal, three diagonal elements ε_{xx}, ε_{yy}, ε_{zz} also exhibit two independent components ($\varepsilon_{xx} = \varepsilon_{yy}$). We note the ε increase with replacement of F by Cl and Br. And the ε_{xx} (ε_{yy}) is larger than the ε_{zz} for Sr-FAP, while for Sr-ClAP and Sr-BrAP, the ε_{xx} (ε_{yy}) is smaller than the ε_{zz} in our calculations.

Taking the calculated macroscopic static dielectric tensor and the Born effective charge tensor into consideration, the long-range coulomb (dipole–dipole) interaction causes the splitting of optical modes at Γ point. The splitting of the LO and TO modes at the Γ point is evident from the phonon dispersion curves that displayed in Fig. 4. The IR vibration frequencies have LO–TO splitting at various frequencies and the LO frequency is larger than the TO frequency. Tables 6 and 7 provide the phonon frequencies of Raman and infrared (including LO–TO splitting) modes, respectively. The comparison between the calculated and the measured frequencies[15,42] gives the maximum deviations of 5.6%, and the frequencies from other groups[39–41] also show good consistency with our calculation. The IR spectra of $Ca_{10}(PO_4)_6F_2$ has been obtained by Etienne Balan *et al.*[11] with DFT, the calculated frequencies underestimate about 10% with respect to the measured IR frequencies. Therefore, the agreement is generally excellent between our calculated and the experimental values. Further analysis, there is a sole Raman active mode E_{2g} which is mainly associated with the atomic vibrations from F atoms according to our calculated phonon partial density of states. In addition, we find the mode A_u (5) which include the vibrations of PO_4 group and Sr, and the mode A_u (8) which correspond to the vibrations of P–O bond exhibit the very large LO–TO splitting (>45 cm^{-1}), indicating these modes are sensitive to the long-range Coulomb interaction.

3.4. Thermodynamic properties

To our knowledge there are some publications focused on the thermodynamic properties of Sr-ClAP, but no experimental or theoretical works exploring the thermodynamic properties of Sr-FAP and Sr-BrAP. As we know that the first-principles for phonon calculations are limited to $T = 0$ K yet the detailed thermodynamic properties of the crystals could be derived by phonons based on the QHA. Neglecting the thermal electronic contributions and focus only the contribution of atomic vibrations, the Helmholtz free energy F of a system at temperature T can be expressed as:

$$F(V_P,T) = E_c(V) + F_{vib}(V,T)$$

where E_c is the static total energy per primitive unit cell at 0 K, and F_{vib} is the vibrational contribution to the Helmholtz free energy F. Under QHA the F_{vib} is defined by

$$F_{vib} = k_B T \int_0^\infty \ln\left\{2 \sinh \frac{\eta\omega}{2k_B T}\right\} g(\omega) d\omega$$

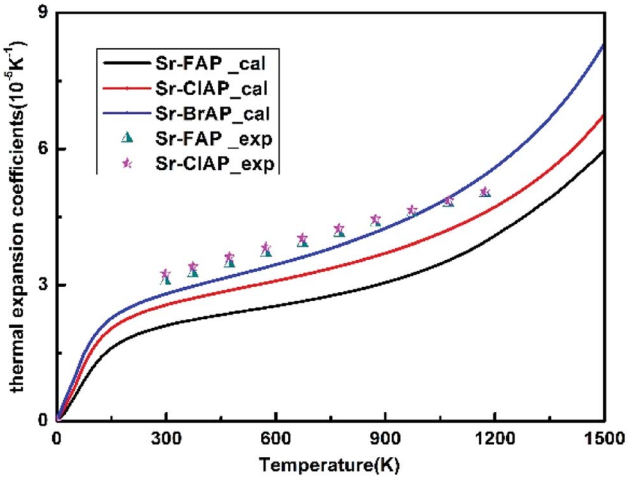

Fig. 6 Thermal expansion coefficient α_V of Sr-FAP, Sr-ClAP and Sr-BrAP apatites as a function of temperature at 0 GPa. Experimental data from ref. 43.

where k_B is the Boltzman constant, ω is the phonon frequencies, $g(\omega)$ is the phonon density of states with $\int_0^\infty g(\omega)d\omega = 3N$.

When the Helmholtz free energy F obtained, the entropy S and internal energy E can be derived by thermodynamic relations, $S = -(\partial F/\partial T)_V$ and $E = F + TS$ respectively. And the heat capacity at constant volume C_V can be estimated directly from Helmholtz free energy by $C_V = -T(\partial^2 F/\partial T^2)_V$. Moreover, the heat capacity at constant pressure C_P which is generally measured in experiments can be calculated using thermodynamic relation: $C_P = C_V + \alpha^2 VBT$, where B is the bulk modulus, V is the volume and α is the volume thermal expansion coefficient. The volume thermal expansion coefficient α is calculated according to the formula $\alpha_V(T) = \frac{1}{V}(\partial V/\partial T)_P$, which is shown in Fig. 6. It is found that our calculated results are smaller than experiment values.[43] One reason is from the fact that the synthetic apatites are polycrystalline and the measurements are conducted at very high temperatures in the experiment, but our calculations are based on ideal single crystal under the 0 K. Another important reason is the neglect anharmonicity and thermal electronic contributions may be the important contributions for these materials.

The predicted thermodynamic properties under different temperature T for $Sr_{10}(PO_4)_6X_2$ (X = F, Cl, Br) are depicted in Fig. 7. The difference of thermodynamic properties for Sr-FAP, Sr-ClAP and Sr-BrAP is small, which is consistent with their similar phonon dispersion curves. From Fig. 7a, it is found the temperature-dependent F shows a decreasing trend from X = F, Cl, to Br. The differences of the temperature-dependent E between these apatites are too small to be observed in Fig. 7b, though a decreasing trend of E is shown from X = F, Cl, to Br. In

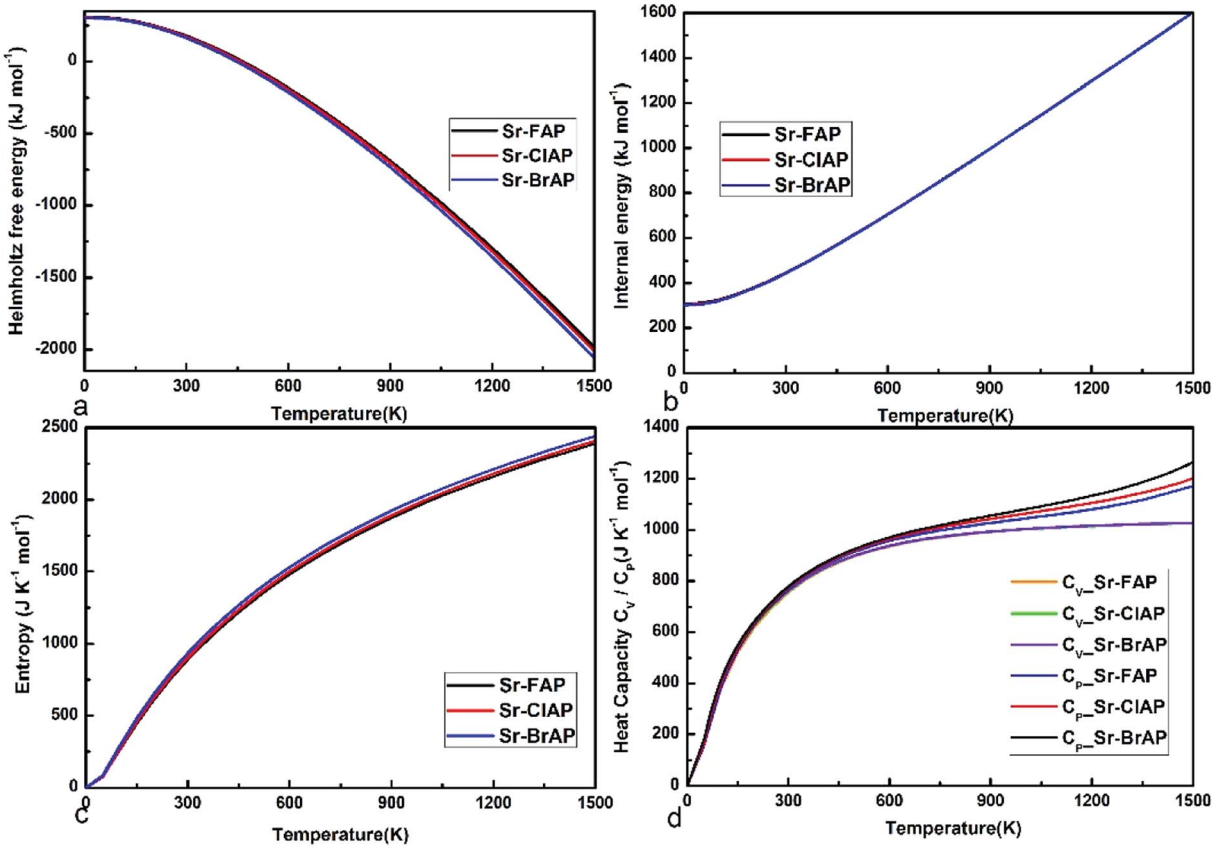

Fig. 7 The thermodynamic properties of Sr-FAP, Sr-ClAP and Sr-BrAP apatites. (a) Helmholtz free energy F, (b) internal energy E, (c) entropy S, (d) specific heat C_V (C_P).

Table 8 The calculated and experimental data of S (J K^{-1} mol^{-1}), $H - H_{298}$ (kJ mol^{-1}), C_P (J K^{-1} mol^{-1}) for Sr-ClAP

	S (J K^{-1} mol^{-1})		$H - H_{298}$ (kJ mol^{-1})		C_P (J K^{-1} mol^{-1})		
T(K)	This work	Expt[a]	This work	Expt[a]	This work	Expt[b]	Expt[a]
0	901	904	0	0	0	—	—
300	906	909	1.52	1.41	773	844	764
400	1138	1153	82.1	86.8	861	995	921
500	1333	1367	169.6	181.8	922	1070	991
600	1500	1551	261.5	283.8	964	1115	1027
700	1647	1711	356.3	387.6	996	1146	1047
800	1776	1852	453.7	492.9	1021	1169	1058
900	1892	1977	552.3	599.0	1042		1064
1000	1997	2089	652.1	705.6	1063		1067
1100	2093	2191	752.7	812.4	1083		1068
1200	2182	2284	854.0	919.2	1105		1068
1300	2263	2369	955.8	1025.9	1130		1066
1400	2339	2448	1058.0	1132.5	1161		1064
1500	2409	2522	1160.5	1238.8	1201		1062

[a] Ref. 49. [b] Ref. 48.

Fig. 7c, S shows a relatively evident increasing trend from X = F, Cl, to Br, which can be explained by the increasing trend of phonon DOSs at the low phonon frequency. Fig. 7d gives the relationships between the specific heat C_V and C_P *versus* temperature that both C_V and C_P exhibit an increasing trend with increasing atom mass (F < Cl < Br) at the given temperature. And with increasing temperature, the both C_V and C_P grow rapidly up to 700 K, then above 700 K, C_P keeps positive slope but C_V tends to be a constant value of 1033 J K^{-1} mol^{-1} that is conform to the well-known Dulong–Petit limit of $C_V = 3nNk_B$ = 1047 J K^{-1} mol^{-1}.

In order to compare our results with the experimental data, Table 8 lists the S, $H - H_{298}$ and C_P at selected temperatures from 298 K to 1500 K for Sr-ClAP. For studies at constant pressure, the appropriate thermodynamic function of enthalpy is $H = E + PV$, where E is the internal energy of the system, P is the pressure, and V is the volume. All our studies are carried out at $P = 0$ GPa and hence $PV = 0$, as a result the $H = E$. It is found the calculated S, $H - H_{298}$ and C_P of Sr-ClAP exhibit reasonable agreement with the experimental values.[35,48,49] So our predicted thermodynamic properties for $Sr_{10}(PO_4)_6X_2$ (X = F, Cl, Br) are reliable. There are no experimental or theoretical works exploring the thermodynamic properties of crystal Sr-FAP and Sr-BrAP for comparison with the present data, we hope our predicted results can give a reference for the future study.

4. Conclusions

In summary, we have done a comprehensive investigations on the structural stability, electronic, vibrational, and thermodynamic properties of the strontium apatites $Sr_{10}(PO_4)_6X_2$ (X = F, Cl, Br) within DFT and DFPT in combination with QHA.

It was observed that with the increase in the size of the c-axis ion ($F^- < Cl^- < Br^-$), the cell volumes of $Sr_{10}(PO_4)_6X_2$ (X = F, Cl, Br) compounds increased, and the optimized structure parameters of $Sr_{10}(PO_4)_6X_2$ (X = F, Cl, Br) are in good agreement with the experimental values. The results of cohesive energies and formation enthalpies show the stability of strontium apatites is related to the anion radius and decreases in the following sequence: Sr-FAP > Sr-ClAP > Sr-BrAP. The electronic structures indicate that strontium apatites $Sr_{10}(PO_4)_6X_2$ (X = F, Cl, Br) are insulator materials with the indirect band gaps, and the band gap values decrease from Sr-FAP, Sr-ClAP, to Sr-BrAP. The detailed vibrational properties are obtained using DFPT. The calculated phonon frequencies are in good agreement with the reported experimental infrared and Raman data in the literatures. According to the calculated phonon dispersions, it is concluded that strontium apatites $Sr_{10}(PO_4)_6X_2$ (X = F, Cl, Br) are dynamically stable, and the phonon behaviors are generally similar for these apatites, but most of the vibrational frequencies decrease from Sr-FAP, Sr-ClAP to Sr-BrAP, which is a consequence of the atomic mass increase ($F^- < Cl^- < Br^-$). The vibrational modes at the gamma point are analyzed from group theory, it is demonstrated that with the replacement of larger Cl^- and Br^- for F^-, all the silent modes B_g, B_u and E_{2u} are affected and the only optically active modes involved is the Raman active mode E_{2g}, which can be explained by the different Wyckoff sites of X (X = F, Cl, Br) ions in theirs apatite structures. From phonon density states, the high-frequency spectra for these selected apatites are naturally very similar, the low frequencies increased with the increase in the atomic mass (F < Cl < Br), and the frequencies in the 300–350 cm^{-1} region are associated with the Sr–F bond only. Some phonon related thermodynamic properties of $Sr_{10}(PO_4)_6X_2$ (X = F, Cl, Br) are predicted from the temperature of 0 to 1500 K and discussed. When the mass of the halogen atoms increase, the entropy S and specific heat C_V and C_P both increase, while free energy F decreases. On the whole, these considered apatites exhibit similar but slightly different behaviors for the thermodynamic properties, which is expected because the halogen atoms F, Cl, Br are in the same VIIA group. Our calculated thermodynamic properties of Sr-ClAP are in reasonable agreement with the experimental values.

We hope that our work could provide a useful guidance for future experimental and theoretical works.

Acknowledgements

This work was financially supported by the National High Technology Research and Development Program of China (2AA034202) and the National Natural Science Foundation of China (No. 11305147).

References

1 K. A. Gross and C. C. Berndt, *Rev. Mineral. Geochem.*, 2002, **48**, 631–672.
2 J. D. Pasteris, *Am. Mineral.*, 2016, **101**, 2594–2610.
3 J. F. Rakovan and J. D. Pasteris, *Elements*, 2015, **11**, 195–200.
4 M. Mathew and S. Takagi, *J. Res. Natl. Inst. Stand. Technol.*, 2001, **106**, 1035.

5 P. H. Mercier, Y. Le Page, P. S. Whitfield, L. D. Mitchell, I. J. Davidson and T. White, *Acta Crystallogr., Sect. B: Struct. Sci.*, 2005, **61**, 635–655.
6 C. Combes, S. Cazalbou and C. Rey, *Minerals*, 2016, **6**, 34.
7 Y. Pan and M. Fleet, *Rev. Mineral. Geochem.*, 2002, **48**, 13–50.
8 J. M. Hughes, M. Cameron and K. D. Crowley, *Am. Mineral.*, 1989, **74**, 870–876.
9 P. Rulis, L. Ouyang and W. Ching, *Phys. Rev. B: Condens. Matter Mater. Phys.*, 2004, **70**, 155104.
10 J. C. Elliott, *Rev. Mineral. Geochem.*, 2002, **48**, 427–453.
11 E. Balan, S. Delattre, D. Roche, L. Segalen, G. Morin, M. Guillaumet, M. Blanchard, M. Lazzeri, C. Brouder and E. K. Salje, *Phys. Chem. Miner.*, 2011, **38**, 111–122.
12 C.-X. Li, Y.-H. Duan and W.-C. Hu, *J. Alloys Compd.*, 2015, **619**, 66–77.
13 A. Slepko and A. A. Demkov, *Phys. Rev. B: Condens. Matter Mater. Phys.*, 2011, **84**, 134108.
14 S. S. Bhat, U. V. Waghmare and U. Ramamurty, *Cryst. Growth Des.*, 2014, **14**, 3131–3141.
15 W. Klee and G. Engel, *J. Inorg. Nucl. Chem.*, 1970, **32**, 1837–1843.
16 Z. Junhui, D. Yonghua, M. Lishi and L. Runyue, *J. Alloys Compd.*, 2016, **680**, 121–128.
17 S. Aryal, K. Matsunaga and W.-Y. Ching, *J. Mech. Behav. Biomed. Mater.*, 2015, **47**, 135–146.
18 Z.-S. Tao, W.-S. Zhou, X.-W. He, W. Liu, B.-L. Bai, Q. Zhou, Z.-L. Huang, K.-k. Tu, H. Li and T. Sun, *Mater. Sci. Eng., C*, 2016, **62**, 226–232.
19 C. Drouet, *J. Chem. Thermodyn.*, 2015, **81**, 143–159.
20 A. P. Soroka, V. L. Karbivskyy and V. H. Kasiyanenko, *Funct. Mater.*, 2015, **22**, 79–92.
21 K. Sudarsanan and R. Young, *Acta Crystallogr., Sect. B: Struct. Crystallogr. Cryst. Chem.*, 1980, **36**, 1525–1530.
22 E. M. Michie, R. W. Grimes, S. K. Fong and B. L. Metcalfe, *J. Solid State Chem.*, 2008, **181**, 3287–3293.
23 A. M. Goryaeva, V. S. Urusov and N. N. Eremin, *Eur. J. Mineral.*, 2013, **25**, 947–955.
24 C. Guo, L. Luan, X. Ding, F. Zhang, F. G. Shi, F. Gao and L. Liang, *Appl. Phys. B: Lasers Opt.*, 2009, **95**, 779–785.
25 M. Kottaisamy, R. Jagannathan, P. Jeyagopal, R. Rao and R. Narayanan, *J. Phys. D: Appl. Phys.*, 2001, **27**, 2210.
26 S. A. Payne, L. D. DeLoach, L. K. Smith, W. L. Kway, J. B. Tassano, W. F. Krupke, B. H. Chai and G. Loutts, *J. Appl. Phys.*, 1994, **76**, 497–503.
27 Q. Wang, S. Zhao, X. Zhang, L. Sun and S. Zhang, *Opt. Commun.*, 1996, **128**, 73–75.
28 C. Wu, J. Zhang, P. Feng, Y. Duan, Z. Zhang and Y. Wang, *J. Lumin.*, 2014, **147**, 229–234.
29 Q. Zeng, H. Liang, G. Zhang, M. D. Birowosuto, Z. Tian, H. Lin, Y. Fu, P. Dorenbos and Q. Su, *J. Phys.: Condens. Matter*, 2006, **18**, 9549.
30 J. Liu, Z.-M. Zhang, Z.-C. Wu, F.-F. Wang and Z.-J. Li, *Mater. Sci. Eng., B*, 2017, **221**, 10–16.
31 P. Marie, *Bone*, 2006, **38**, 10–14.
32 J. F. Rakovan and J. M. Hughes, *Can. Mineral.*, 2000, **38**, 839–845.
33 C. Wu, Y. Ramaswamy, D. Kwik and H. Zreiqat, *Biomaterials*, 2007, **28**, 3171–3181.
34 W. Zhang, Y. Shen, H. Pan, K. Lin, X. Liu, B. W. Darvell, W. W. Lu, J. Chang, L. Deng and D. Wang, *Acta Biomater.*, 2011, **7**, 800–808.
35 B. K. Maji, H. Jena, M. Krishnaiah and R. Asuvathraman, *J. Therm. Anal. Calorim.*, 2016, **124**, 857–863.
36 S. H. Swafford and E. M. Holt, *Solid State Sci.*, 2002, **4**, 807–812.
37 K. Sudarsanan and R. Young, *Acta Crystallogr., Sect. B: Struct. Crystallogr. Cryst. Chem.*, 1974, **30**, 1381–1386.
38 P. Alberius-Henning, C. Mattsson and S. Lidin, *Z. Kristallogr. - New Cryst. Struct.*, 2000, **215**, 345–346.
39 A. Aissa, B. Badraoui, R. Thouvenot and M. Debbabi, *Eur. J. Inorg. Chem.*, 2004, **2004**, 3828–3836.
40 S. Zhai, S. R. Shieh, W. Xue and T. Xie, *Phys. Chem. Miner.*, 2015, **42**, 579–585.
41 C. E. Bonner, C. C. Chess, C. Meegoda, S. Stefanos and G. B. Loutts, *Opt. Mater.*, 2004, **26**, 17–22.
42 A. Schulte, S. C. Buchter and B. H. Chai, *International Society for Optics and Photonics*, 1995, **2380**, 34–42.
43 N. Chernorukov, A. Knyazev and E. Bulanov, *Inorg. Mater.*, 2011, **47**, 172–177.
44 A. V. Knyazev, N. G. Chernorukov and E. N. Bulanov, *Mater. Chem. Phys.*, 2012, **132**, 773–781.
45 M. Jemal, A. B. Cherifa, I. Khattech and I. Ntahomvukiye, *Thermochim. Acta*, 1995, **259**, 13–21.
46 I. Khattech and M. Jemal, *Thermochim. Acta*, 1997, **298**, 23–30.
47 I. Khattech and M. Jemal, *Thermochim. Acta*, 1997, **298**, 17–21.
48 R. V. Krishnan, H. Jena, K. G. Kutty and K. Nagarajan, *Thermochim. Acta*, 2008, **478**, 13–16.
49 R. Babu, H. Jena, K. G. Kutty and K. Nagarajan, *Thermochim. Acta*, 2011, **526**, 78–82.
50 M. Kocher, A. Jain, S. P. Ong and G. Hautier, Materials Project, https://www.materialsproject.org/materials/mp-6669, mp-23121, mp-23141.
51 J. A. L. Rabone and N. De Leeuw, *J. Comput. Chem.*, 2006, **27**, 253–266.
52 W. Kohn and L. J. Sham, *Phys. Rev.*, 1965, **140**, A1133.
53 G. Kresse and J. Furthmüller, *Phys. Rev. B: Condens. Matter Mater. Phys.*, 1996, **54**, 11169.
54 D. M. Ceperley and B. Alder, *Phys. Rev. Lett.*, 1980, **45**, 566.
55 H. J. Monkhorst and J. D. Pack, *Phys. Rev. B: Condens. Matter Mater. Phys.*, 1976, **13**, 5188.
56 A. Togo and I. Tanaka, *Scr. Mater.*, 2015, **108**, 1–5.
57 K. Momma and F. Izumi, *J. Appl. Crystallogr.*, 2011, **44**, 1272–1276.
58 P. V. Balachandran, K. Rajan and J. M. Rondinelli, *Acta Crystallogr., Sect. B: Struct. Sci., Cryst. Eng. Mater.*, 2014, **70**, 612–615.
59 Y. Wang, S.-L. Shang, H. Fang, Z.-K. Liu and L.-Q. Chen, *npj Comput. Mater.*, 2016, **2**, 16006.
60 S. Baroni, S. De Gironcoli, A. Dal Corso and P. Giannozzi, *Rev. Mod. Phys.*, 2001, **73**, 515.
61 X. Gonze and C. Lee, *Phys. Rev. B: Condens. Matter Mater. Phys.*, 1997, **55**, 10355.